minerals

MDPI

Article

Characterization of Compacted Ca- and Na-Bentonite with Copper Corrosion Products in the KAERI Underground Research Tunnel

Mihye Kong *, Minsoo Lee, Gha-Young Kim, Junhyuk Jang and Jin-Seop Kim

Disposal Performance Demonstration Research Division, Korea Atomic Energy Research Institute, 111, Daedeok-daero 989 beon-gil, Yuseong-gu, Daejeon 34057, Republic of Korea; minm@kaeri.re.kr (M.L.); gkim@kaeri.re.kr (G.-Y.K.); jangjunhyuk@kaeri.re.kr (J.J.); kjs@kaeri.re.kr (J.-S.K.)
* Correspondence: mhkong@kaeri.re.kr; Tel.: +82-42-868-2030

Abstract: In a deep geological disposal system, bentonite buffer material is an important barrier used to protect the disposal canister from the inflow of groundwater and prevent the outflow of radionuclides. This study aimed to characterize the mineralogical and chemical reactions of bentonite caused by copper corrosion of the canister in a radioactive waste repository. We investigated the d-spacings of montmorillonite in Gyeongju bentonite (Ca-type, KJ-I) under groundwater-saturated conditions over 10 years and compared their characteristics with those of Wyoming bentonite (Na-type, MX-80) in the Korea Atomic Energy Research Institute Underground Research Tunnel. Mineralogical investigations using X-ray diffraction and focused ion beam energy-dispersive spectroscopy indicated that no transformation of smectite or neo-formed clay phases occurred. In the Ca-type bentonite (KJ-I), the swelling was observed when it was in contact with rolled plate (RP) and cold-spray-coated (CSC) copper, with d-spacing expansions of 2.9% and 3.8%, respectively. In contrast, the Na-type bentonite (MX-80) showed d-spacing expansions of 17.6% and 19.6% when it was in contact with the RP and CSC Cu, respectively. The Cu concentration and distribution indicated that the corrosion products dissolved and then diffused into the surrounding bentonite, with maximum penetration depths of 2.0 and 0.5 mm over 10 years, respectively.

Keywords: bentonite buffer; d-spacing; copper canister corrosion product; penetration depth; KURT

Citation: Kong, M.; Lee, M.; Kim, G.-Y.; Jang, J.; Kim, J.-S. Characterization of Compacted Ca- and Na-Bentonite with Copper Corrosion Products in the KAERI Underground Research Tunnel. *Minerals* **2023**, *13*, 898. https://doi.org/10.3390/min13070898

Academic Editor: Gianvito Scaringi

Received: 7 June 2023
Revised: 24 June 2023
Accepted: 28 June 2023
Published: 30 June 2023

1. Introduction

The core concept of deep geological disposal is to prevent the leakage of radionuclides for several thousands of years using a disposal canister and then to delay the movement of the radionuclides using engineered and natural barriers including buffer materials. To dispose of high-level radioactive waste via deep geological disposal, buffer materials that can act as a buffer against external factors, such as the intrusion of groundwater and earthquakes, and metal canisters that can cover high-level spent fuel rods are required [1,2]. The buffer material filled between the disposal canister and the hole in a deep geological disposal system fixes the disposal canister to the hole and protects it from physical impacts, such as the shearing behavior of the surrounding rock and oxidizing agents such as oxygen or hydrogen sulfide that could corrode the disposal canister. Furthermore, it serves as an intrusion prevention system. In addition, even if the disposal canister loses airtightness and radionuclides are leaked, the buffer can slow or even immobilize their diffusion [3].

Buffer materials acting as a barrier for a repository should have a high swelling property that can fix the disposal canister during external vibrations without shaking, low hydraulic conductivity to suppress the material's movement, and high ion adsorption power to immobilize metal ions in the form of cations. Additionally, it should have a low organic matter content to inhibit the growth of microorganisms and high thermal conductivity to dissipate heat from the disposal canister [2,4–9]. Therefore, it is important

to ensure that these properties are preserved under real repository conditions for hundreds of thousands of years.

Bentonite is divided into Ca- and Na-type bentonite according to the species of exchangeable cations present between the layers, and volume expansion is achieved via swelling through interlayer hydration [10–14]. The swelling ability of bentonite acts as a seal of the space between the disposal canister and disposal hole and blocks the inflow of groundwater from the surrounding host rock [15]. Upon closure of the repository, the surrounding bentonite is gradually saturated with the influx of natural porewater from the surrounding parent rock, while simultaneously experiencing a temperature rise owing to the radioactive decay of the waste [3,7,16].

As copper (Cu) canister corrosion occurs, mobile dissolved Cu species are released through the reaction with the bentonite buffer [7,17]. The mechanism and corrosion products of corrosion reactions in the disposal canister change as the disposal environment evolves, and the resulting corrosion products may remain in the form of sediments at the interface between the disposal canister and buffer or penetrate the buffer via transformation, resulting in changes in buffer performance.

Under aerobic conditions, Cu corrosion is dominated by chloride ions, and when Cu is oxidatively dissolved, oxygen is reduced to produce OH^-. Cu does not dissolve directly into Cu(II) in the Cl^- solution but exists as $CuCl_2^-$ and remains a major chemical species in the repository area, even after 10,000 years [18,19]. Corrosion reactions in anaerobic environments are dominated by sulfide (HS^-) [20]. When HS^- is present at the interface of the Cu canister, Cu is dissolved in the form of a CuS_2 precipitate. This corrosion reaction is accompanied by HS^- or H_2O reduction reactions to produce H_2. Cu_2O produced under aerobic conditions reacts with HS^- and is converted into Cu_2S. The Cu corrosion rate under anaerobic conditions is governed by HS^- mass transfer [8,21,22]. The present study was conducted under aerobic conditions, and S concentration was measured (Table 1).

Table 1. S concentration of KJ-I, MX-80, and bentonite in contact with copper (Cu) materials (rolled plate [RP] and cold-spray-coated [CSC] Cu).

Samples Oxides (wt%)	KJ-I	MX-80	RP Cu		CSC Cu	
			Ca-B	Na-B	Ca-B	Na-B
S (wt%)	1.76 (μg/mL)	<0.24				

The Korea Atomic Energy Research Institute (KAERI) has been developing copper canisters using a low-temperature spray-coating technique for the disposal of high-level nuclear waste. We intended to examine the long-term corrosion behavior of the canister materials at 30 °C. This study aims to understand the interaction of bentonite buffer in contact with a cold-spray-coated (CSC) Cu canister for use as a high-level radioactive waste disposal canister by investigating the chemical and mineralogical changes in Ca- and Na-type bentonite caused by corrosion products.

2. Materials and Methods

2.1. Sample

The buffer material was manufactured as a compressed block using two types of bentonite: Ca-type Gyeongju bentonite (i.e., KJ-I) and Na-type Wyoming bentonite (i.e., MX-80) (water content of approximately 11–12 wt%). The dry density of the bentonite block was approximately 1.6 g/cm^3; it had a swelling pressure of approximately 5–7 MPa at room temperature (25 °C) and a hydraulic conductivity of 7.6×10^{-14} m/s [23]. The compressed block was cylindrical, with a diameter of 30 mm and a height of 10 mm. The upper plate was also cylindrical, and the lower plate had a groove in the center, which was 15 mm in diameter and 1.0 mm in depth so that a metal specimen could be inserted.

The bentonite used in this experiment was produced at a mine in Yangnam-myeon, Gyeongju, South Korea. Currently, most of the bentonite mined outdoors in Korea is Ca-type bentonite, and Gyeongju bentonite, which is relatively rich in montmorillonite (approximately 60%), has been proposed as a standard buffer material for high-level waste repositories. As of 2015, KAERI has been conducting research with the bentonite used in the previous test (KJ-I) and the new bentonite used subsequently (KJ-II). However, as Gyeongju bentonite is no longer produced, the new bentonite, which has been researched since 2022, is named Bentonil-WRK. The Gyeongju bentonite used in this experiment was KJ-I. Na-type Wyoming bentonite, with a montmorillonite content of approximately 80%, was purchased from a commercial source.

The Cu specimens were CSC and rolled plate (RP) Cu. For the CSC Cu, the specimen was processed so that the coating obtained via the cold spray coating of domestic Changseong copper powder (purity 99.5 wt%, oxygen content 0.41 wt%) on the cast iron surface appeared coin-shaped, parallel to the coating surface. The cold-spray-coating conditions were as follows: the main injection gas temperature was 600 °C, the powder preheating temperature was 400 °C, and the injection pressure was 30 bar. Commercially available rolled Cu plates were used.

2.2. Corrosion Cell Using the Long-Term In Situ Experiment

Using the Advanced-Korea Reference disposal system for spent nuclear waste (A-KRS) developed by KAERI, a unit corrosion experiment cell for the KAERI Underground Research Tunnel (KURT) long-term test was constructed, as shown in Figure 1. A coin-type Cu specimen was positioned at the center between two compact bentonite blocks and was inserted into a titanium test cell. The Cu specimen represents the disposal canister, the compact bentonite block represents the buffer material, and the titanium test cell represents the borehole at the underground bedrock.

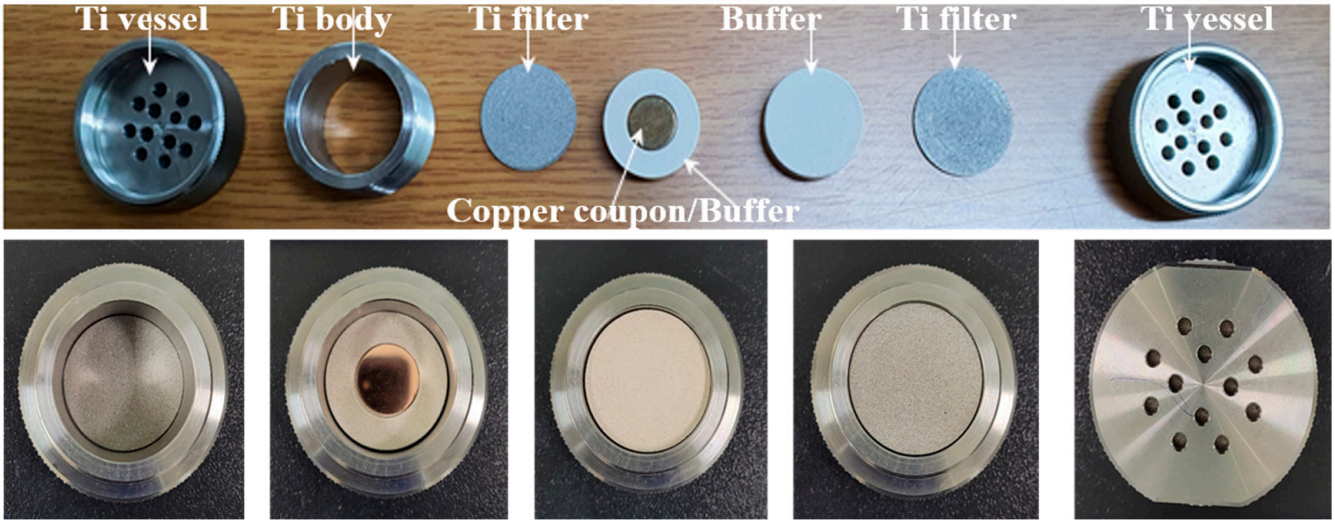

Figure 1. Assembly of the long-term cell in situ.

The test cell consists of a short body tube with a male threaded through both ends and two female screw caps blocking both ends of the body tube. In addition, each cap has 12 holes with a 3.0 mm diameter so that external water can permeate through the cell. Titanium filters with a pore size of 10 μm were placed on both sides to prevent the internal compact bentonite buffer from escaping through the perforated hole. Using this cell, the experiment was conducted over 10 years under aerobic conditions at KURT.

2.3. KURT Groundwater

Groundwater that was naturally ejected from the exploration well at a depth of approximately 150 m from KURT RG-1 was supplied to the chamber via groundwater pressure alone, without using a separate pump. As the groundwater pressure varies depending on the season, groundwater was supplied to the chamber through a water tank at a certain height to maintain a constant water pressure. The flow rate of the groundwater was kept constant at approximately 10–20 mL/min by controlling the valve attached to the chamber outlet. The amount of dissolved oxygen in the supplied groundwater was 4–6 mg/L, and in the case of the 30 °C chamber used in this experiment, the amount was measured to be approximately 3.0–4.5 mg/L. The hydrogen ion concentration was weakly alkaline (pH 8.5), and the oxidation–reduction potential was between 100 and 200 mV. The ion concentrations in the KURT groundwater were 8.2 ppm for Na, 0.48 ppm for K, 19 ppm for Ca, 1.4 ppm for Mg, 9.6 ppm for Si, N.D. for Al and Fe, 3.1 ppm for Cl^-, 1.9 ppm for F^-, 10 ppm for $NO_3{}^-$, and 4.3 ppm for $SO_4{}^{2-}$.

2.4. Geochemical Analysis of Solid Samples

Inductively coupled plasma atomic emission spectroscopy (ICP-AES) and X-ray fluorescence spectroscopy (XRF) were used to analyze the chemical composition of the bentonite in contact with Cu. Samples were taken 0.5 mm from the surface of the bentonite block in contact with the Cu corrosion specimen, and the major cations were quantitatively analyzed via ICP-AES according to thickness. The major compounds (SiO_2, Al_2O_3, Fe_2O_3, CaO, MgO, K_2O, Na_2O, TiO_2, MnO, and P_2O_5 in %) were analyzed using an XRF spectrometer from Shimadzu, Korea Institute of Geoscience and Mineral Resources (KIGAM). The major elements (Ca, Na, Fe, K, Cu) were measured using ICP-AES (I-CAP Q, Göteborg, Sweden, KBSI Ochang center).

2.5. Mineralogical Analysis

The sealing properties of a buffer material are closely related to the interactions between montmorillonite and water [23]. Therefore, mineral analysis is necessary to determine the montmorillonite content and swelling capacity. The composition and distribution of minerals are known to influence the long-term geochemical evolution of buffer materials.

The bentonite in contact with Cu was analyzed using X-ray diffraction (XRD) at the KIGAM, and the mineral composition and content were analyzed using the SIROQUANT v4.0 program. The XRD pattern was obtained from random powders using a Philips X'Pert-PRO MPD diffractometer and an anticathode Cu-Kα (λ = 1.54 Å) at 40 kV and 30 mA. The samples were analyzed from 3° to 65° 2θ with a step size of 0.01° 2θ. The scan rate per step was 0.04 s.

2.6. Cu Corrosion Analysis

Focused ion beam (FIB) scanning electron microscopy (SEM) and energy-dispersive X-ray spectroscopy (EDS) were performed using a ZEISS Crossbeam 540 equipped with the Bruker EDS system at Chungbuk National University (Oberkochen, German, Center for Research Facilities).

3. Results

3.1. Cu Corrosion

The surface of the compacted KJ-I and MX-80 contained Cu corrosion products. The possible chemical interaction between the corrosion products and bentonite indicated that the Cu was most likely present as Cu^{2+} ions. Interactions between the Cu^{2+} ions and the various bentonite components might thus include precipitation (with anions in the pore water), adsorption on the outer montmorillonite surfaces, and diffusion into the interlamellar montmorillonite spaces or in the free water between the bentonite particles.

Figures 2 and 3 show the SEM-EDS and mapping results of the FIB-prepared specimens. Cu-rich corrosion products appear as bright areas in the SEM images, caused by electron

density differences. These results indicate that the corrosion and penetration of Cu into the bentonite were heterogeneous on a μm–mm scale. Figure 2A,C shows the corrosion-product-dependent bentonite of the measured FIB-SEM images of Ca-bentonite (KJ-I) in contact with the RP and CSC Cu. In the Ca-bentonite in contact with the RP Cu, Cu_2O was present in the intermediate layer at a thickness of approximately <1 μm. In the Ca-bentonite in contact with the CSC Cu, CuO compounds were distributed in the upper layer, and approximately 16.9 μm of the Cu_2O and Cu metal was distributed in the middle layer (Figure 2). On the other hand, the Cu metal in the middle area and CuO compound in the upper layer were distributed in the Na-bentonite in contact with the RP and CSC Cu, and Cu_2O was absent. Overall, the ICP-AES data showed that fewer Cu corrosion products were produced for Na-bentonite than for Ca-bentonite (Figure 4).

Increased Cu concentrations were found at the interface of bentonite-Cu material (e.g., canister), probably indicating Cu corrosion. The changes in Cu concentration analyzed based on the RP and CSC Cu thickness are shown in Figure 4 for the Ca- and Na-bentonite. In the Ca-bentonite with RP and CSC Cu corrosion products, the concentration of Cu cations dissolved from the Cu materials increased (approximately 0.99% and 2.46%) with proximity to the surface in contact with Cu materials. However, the Cu concentration decreased to that found 2 mm from the interface. In particular, the Cu cation concentration was 2.5 times higher in the CSC Cu than in the RP Cu. This is consistent with the corrosion thickness difference (3.94 μm for RP and 6.28 μm for CSC Cu) obtained using the weight loss method.

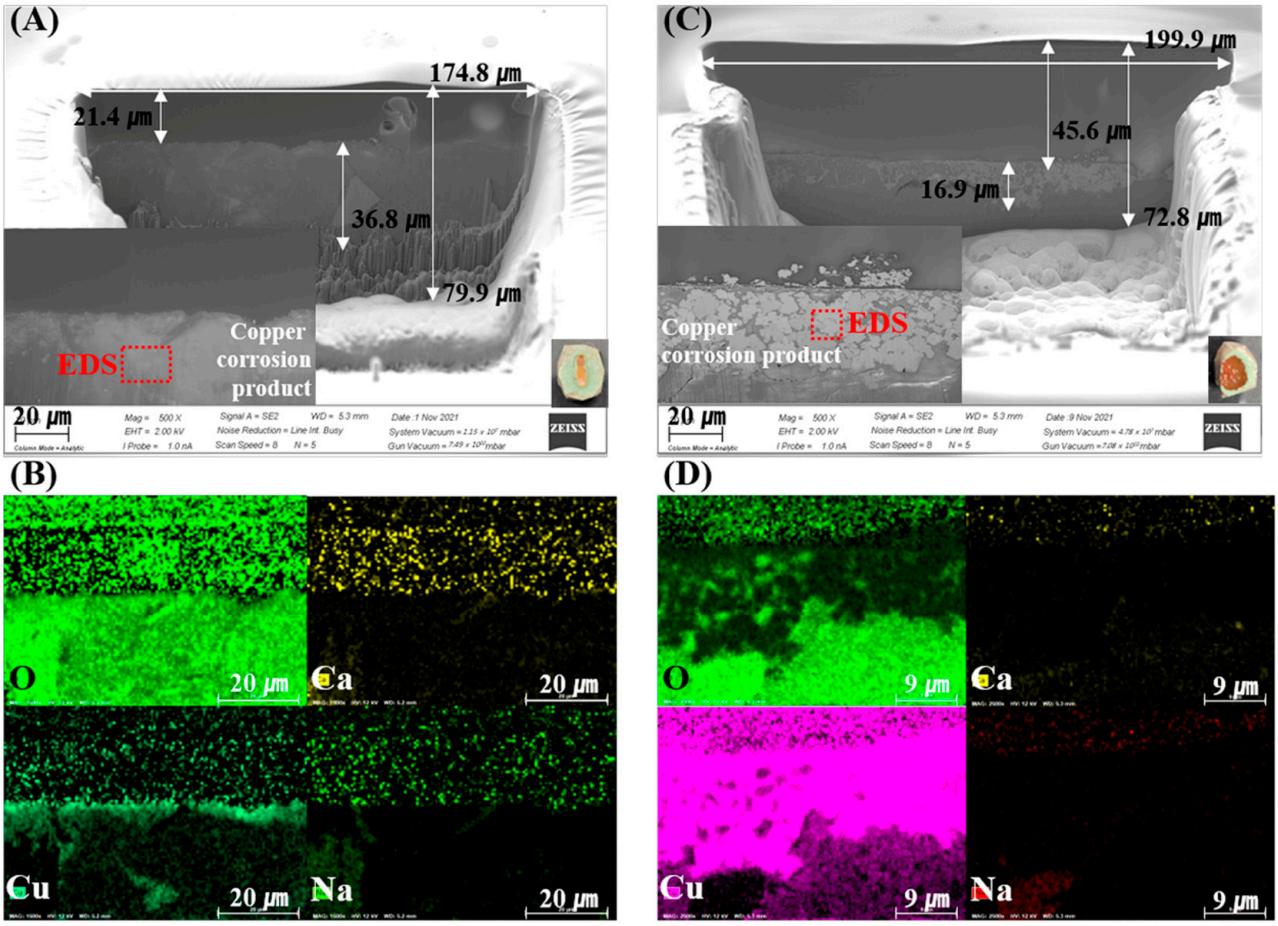

Figure 2. Scanning electron microscopy (SEM) images of the focused ion beam (FIB) cross-sections of the Ca-bentonite (KJ-I) surface in contact with the corrosion products of rolled plate (RP) Cu (**A**) and cold-spray-coated (CSC) Cu (**C**) at 30 °C over 10 years. (**B**,**D**) Oxygen, calcium, copper, and sodium maps.

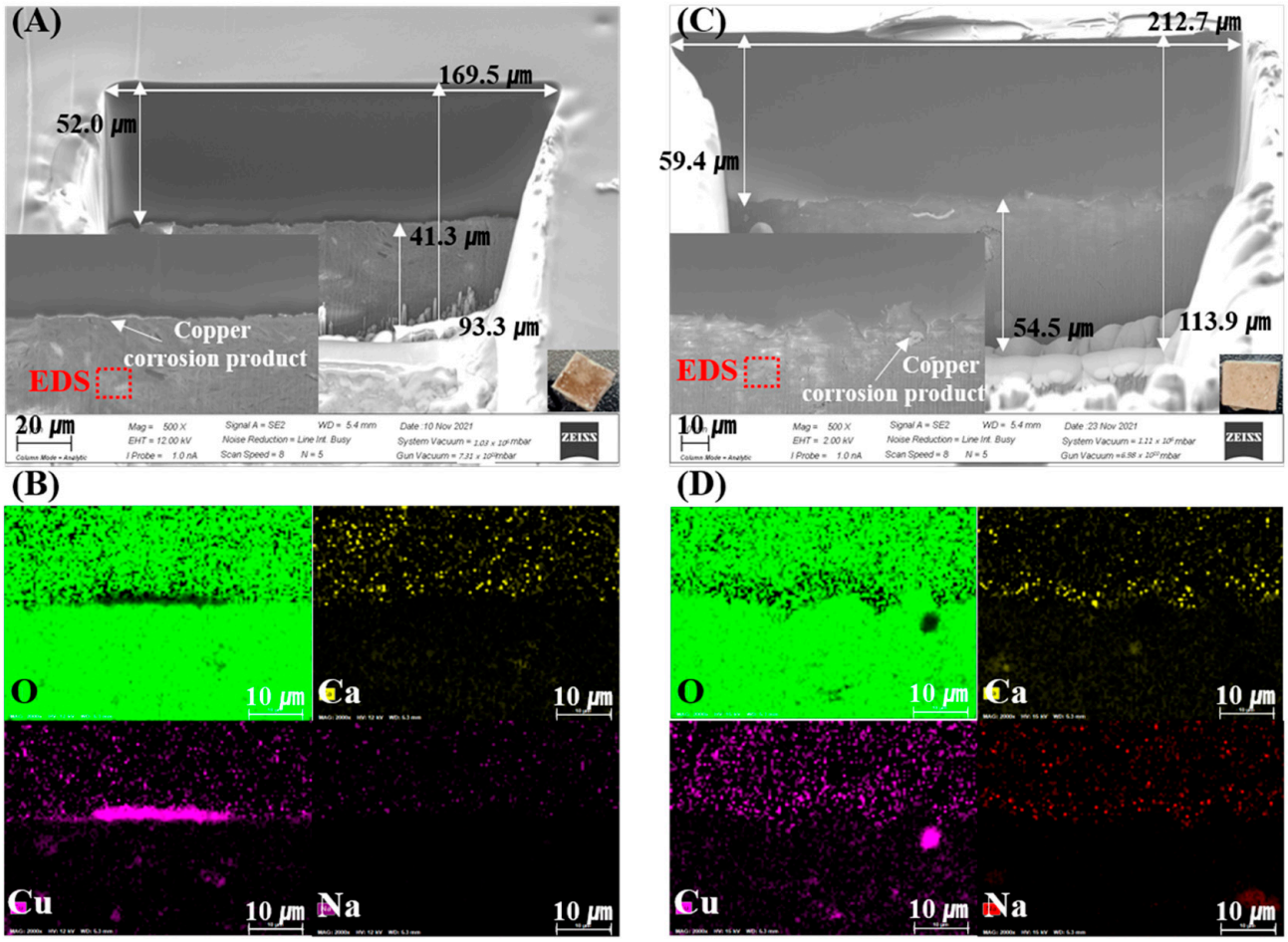

Figure 3. Scanning electron microscopy (SEM) images of the focused ion beam (FIB) cross-sections of the Na-bentonite (MX-80) surface in contact with the corrosion products of rolled plate (RP) Cu (**A**) and cold-spray-coated (CSC) Cu (**C**) at 30 °C over 10 years. (**B**,**D**) Oxygen, calcium, copper, and sodium maps.

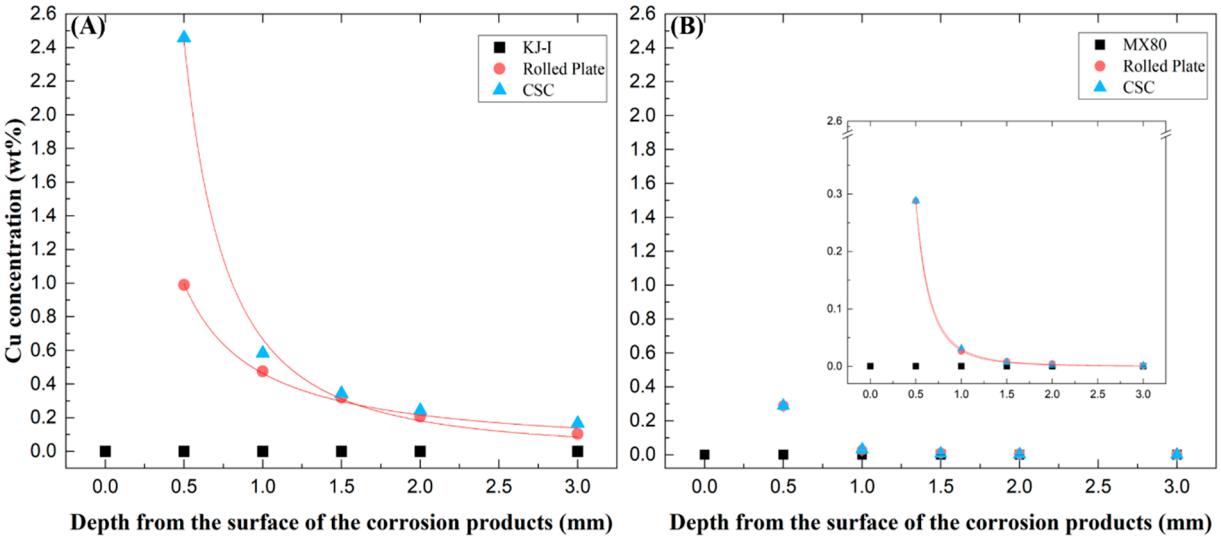

Figure 4. The concentration of copper (Cu) as a function of depth from the surface of the compacted Ca- (**A**) and Na-bentonite (**B**) blocks with corrosion products (rolled plate (RP) and cold-spray-coated (CSC) Cu) via inductively coupled plasma atomic emission spectroscopic analysis.

On the other hand, in the Na-bentonite with RP and CSC Cu corrosion products, the concentration of Cu cations dissolved in the two materials was the same (approximately 0.29%) and appeared higher and closer to the surface in contact with the Cu materials. However, the Cu cations were concentrated within 0.5 mm and did not diffuse beyond a 1 mm depth. Further away from the corrosion surface, both profiles dropped to values close or equal to zero.

3.2. Geochemistry of the Solid Samples

The chemical compositions of the initial Ca-type bentonite (KJ-I) and Na-type bentonite (MX-80) in contact with Cu materials over 10 years are shown in Table 1. Notably, the concentration of CaO in KJ-I increased from 2.59% to 3.37% (RP Cu) and 3.31% (CSC Cu), and that of Na_2O increased from 1.25% to 1.78% (RP Cu) and 1.76% (CSC Cu). Furthermore, in MX-80, the concentration of CaO increased from 1.49% to 2.81% (RP Cu) and 2.83% (CSC Cu), whereas that of Na_2O decreased from 2.25% to 0.42% (RP Cu) and 0.41% (CSC Cu) (Table 2). These results suggest that changes in CaO and Na_2O concentrations are due to cation exchange between corrosion products and bentonite and groundwater or mineral dissolution. The smectite surface has a high affinity for Cu(II). Therefore, the corrosion products generated when the Cu disposal canister is corroded migrate to the bentonite through diffusion and are then adsorbed on the bentonite.

Table 2. Chemical composition of KJ-I, MX-80, and bentonite in contact with copper (Cu) materials (rolled plate [RP] and cold-spray-coated [CSC] Cu).

Samples Oxides (wt%)	KJ-I *	MX-80	RP Cu		CSC Cu	
			Ca-B	Na-B	Ca-B	Na-B
SiO_2	56.80	63.93	63.59	63.76	63.92	64.13
Al_2O_3	19.96	18.49	15.79	17.73	15.78	17.72
Fe_2O_3	6.03	4.09	3.39	3.93	3.40	3.94
CaO	2.59	1.49	3.37	2.81	3.31	2.83
MgO	0.77	2.45	3.04	2.49	3.03	2.46
K_2O	0.93	0.59	0.83	0.55	0.82	0.56
Na_2O	1.25	2.25	1.78	0.42	1.76	0.41
TiO_2	0.83	0.20	0.37	0.19	0.38	0.19
MnO	0.04	0.02	0.05	0.02	0.04	0.02
P_2O_5	0.11	0.06	0.08	0.07	0.08	0.07
FeO	0.15	-	-	-	-	-
Total, % (without Ig.loss)	89.46	93.57	92.29	91.97	92.52	92.33
Ig.loss	9.17	6.15	7.33	7.76	6.94	7.27

* Existing literature [5] measurements are cited.

3.3. Mineralogy

The locations where Cu is sorbed are between the interlayer site in the bentonite and the edge site [24–27]. In the case of the former, an outer surface complex is generated via a reversible cation exchange reaction. Figure 5 shows the Cu-material-dependent changes in the measured XRD patterns of the Ca-bentonite (KJ-I) and Na-bentonite (MX-80) in contact with RP and CSC Cu under KURT groundwater-saturated conditions. The broadness and position of the (001) peak of Ca-bentonite (KJ-I) changed. For comparison, the position of the (001) peak of Na-bentonite (MX-80) changed, and the appearance of a shoulder was observed. This indicates that the interlayer Na^+ in the Na-bentonite was easily exchanged with other ions [28]. In contrast, when Cu is sorbed at the edge site, the inner surface complex is formed through the complex's formation, which is not desorbed even when treated with a weak acid. The chemical properties of adsorbed Cu vary with the pH, Cu concentration, ionic strength, electrolyte composition, and experimental time [27]. Lee et al. [29] reported that some characteristic ion exchange and cation release phenomena occur in the bentonite clay interacting with aqueous Cu cations. Therefore,

XRD was used to determine whether the presence of Cu in the bentonite could affect the interlamellar spacing of the montmorillonite or the types of solids present. The six diffractograms obtained exhibited no differences in mineral composition, indicating that Cu^{2+} was present in quantities that were too small to have any detectable physicochemical effects. The main constituent minerals were montmorillonite (C2/m(12), #13–0135), quartz (P3221(154), #79–1910), cristobalite (P41212(92), #11–0695), albite($C\bar{1}$(15), #71–1150), and calcite ($R\bar{3}c$(161), #83–0578). The mineral composition showed no significant differences between the reference materials.

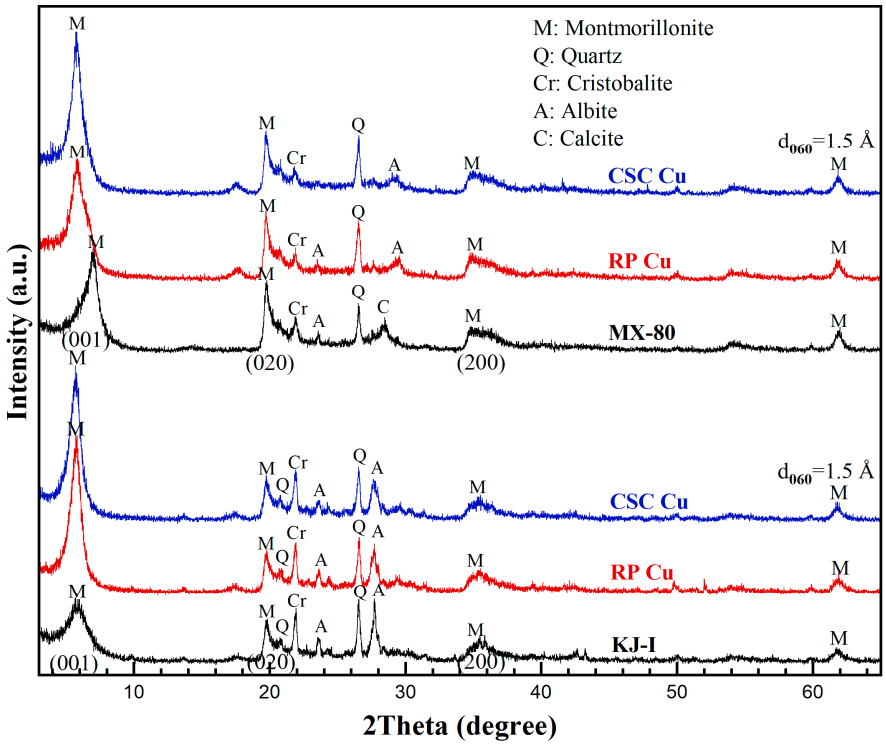

Figure 5. Changes in the X-ray powder diffraction patterns of Gyeongju bentonite (KJ-I) and Wyoming bentonite (MX-80) in contact with copper materials. Rolled plate Cu: RP Cu. Cold-spray-coated Cu: CSC Cu. M: montmorillonite, Q: quartz, Cr: cristobalite, A: albite, C: calcite.

To compare the behaviors of the Ca-bentonite (KJ-I) and Na-bentonite (MX-80) with Cu corrosion products, Figure 6 shows the calculated and normalized d-spacings of the (001) peak of montmorillonite. In the stacked graph (Figure 6b), the $d_{(001)}$ distance of the montmorillonite changed as a function of the Cu materials. KJ-I, the initial bentonite, showed a $d_{(001)}$ distance of 14.9861(1) Å, which is normally observed for bentonites under initial conditions. For the KJ-I mixed with RP Cu, $d_{(001)}$ changed to 15.4258(1) Å, showing a 2.9% increase in the d-spacing. For KJ-I mixed with CSC Cu, $d_{(001)}$ increased continuously from 15.4258(1) to 15.5278(1) Å. MX-80 showed a $d_{(001)}$ spacing of 12.7727(1) Å. When mixed with RP Cu, the $d_{(001)}$ changed dramatically to 14.9562(1) Å, exhibiting a 17.6% increase in the d-spacing. When mixed with CSC Cu, $d_{(001)}$ increased steadily from 14.9562(1) to 15.2449(1) Å. Finally, the d-spacings of KJ-I and MX-80 increased by 3.6% and 19.4%, respectively.

In KJ-I, the contents of the montmorillonite in contact with the RP and CSC Cu were approximately 59.5% and 59.3%, respectively. In MX-80, the contents of montmorillonite in contact with the RP Cu and CSC Cu were 76.7% and 76.0%, respectively. Major minerals other than montmorillonite were confirmed: albite, quartz, cristobalite, calcite, and heulandite (Table 3). As the minerals in an underground disposal environment gradually transition owing to geochemical reactions in the long term, their characteristics and roles must also be examined from a long-term perspective.

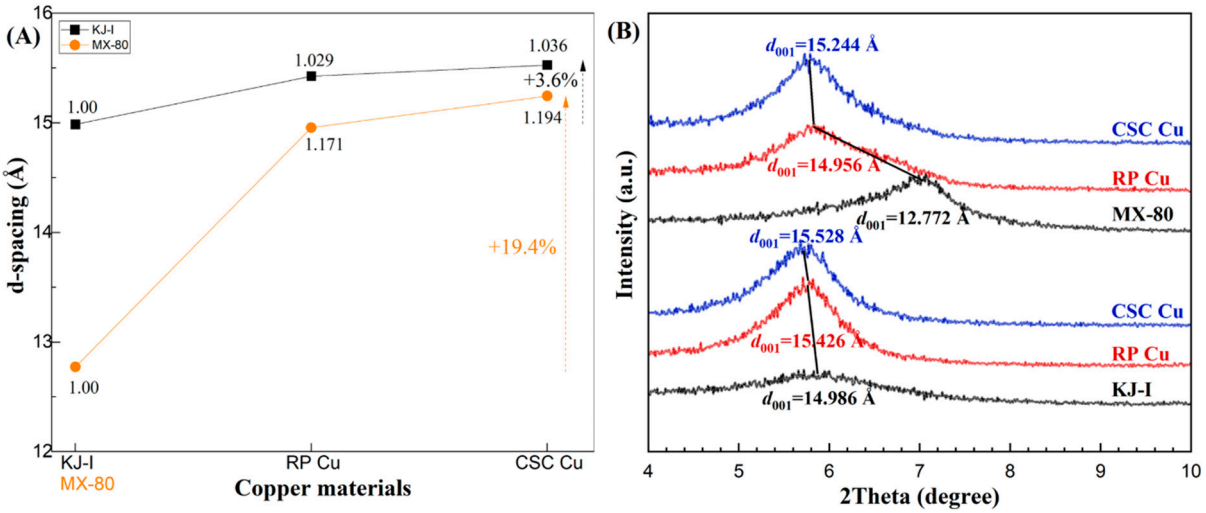

Figure 6. The d-spacing (Å) of montmorillonite (001) reflections as a function of copper (Cu) materials. (**A**) The black squares show the calculated d-spacings of KJ-I in contact with rolled plate (RP) Cu and cold-spray-coated (CSC) Cu, and the orange circles show those of MX-80. (**B**) Corresponding detailed changes in the X-ray diffraction patterns of the (001) peak for KJ-I and MX-80 are shown for contact with copper materials over 10 years. Changes in the interlayer basal distances, $d_{(001)}$, are shown with black lines.

Table 3. Quantitative analysis of minerals, excluding montmorillonite, in the KJ-I, MX-80, and bentonite in contact with copper (Cu) materials.

Minerals	Volume (%)					
	KJ-I *	MX-80	Rolled Plate Cu		CSC	
			Ca-Type Bentonite	Na-Type Bentonite	Ca-Type Bentonite	Na-Type Bentonite
Albite	25.6	10.3	23.5	7.4	23.0	7.4
Quartz	4.9	6.7	9.8	11.2	9.8	11.0
Cristobalite	3.0	3.3	5.0	4.6	5.9	5.7
Calcite	2.1	1.5	2.2	-	2.0	-
Heulandite †	1.8	miner	miner	-	miner	-

* The existing literature [30] is cited. † C2/m(12).

4. Discussion

In this study, a field experiment was conducted to confirm whether the performance and characteristics of bentonite buffer materials surrounding a Cu disposal container for high-level waste disposal are maintained in the long term following the corrosion of the candidate materials in a deep geologic environment. After 10 years of operation, the corrosion cell in the KURT in situ aerobic experiment was dismantled. The chemical and mineralogical properties of Ca- and Na-type bentonite in contact with Cu materials, such as RP and CSC Cu, were characterized using FIB-SEM-EDS, ICP, XRF, and XRD measurements. The d-spacing expansion of montmorillonite is directly associated with the swelling ability of the buffer material. Based on the d-spacing value, it can be seen whether the buffer can be substituted with Ca, Na, or other cations (such as Cu) and how many water layers are combined. Based on this, it can be determined whether the performance of the buffer material as an engineered barrier is maintained.

The penetration thicknesses of the resulting corrosion products in the Ca- and Na-bentonite were up to 2.0 and 0.5 mm over 10 years, with penetration rates of 0.2 and 0.05 mm/year, respectively. As the disposal environment evolves, the resulting corrosion products also change. The difference in penetration depth between the two bentonites may be due to various complex factors. The hydraulic conductivity of Na-bentonite (10^{-13} to

10^{-14} m/s) [31] is lower than that of Ca-bentonite (10^{-12} to 10^{-13} m/s) [5], which affects the diffusion of corrosion products. Furthermore, because Na-bentonite has a low layer charge (<0.425 e/h.u.c., i.e., electrons per half unit cell) and a high viscous suspension [32,33], the penetration of the corrosion products is considered to be lower than that of Ca-bentonite with a high layer charge (>0.475 e/h.u.c.). Corrosion products may be present in the form of precipitates on the surfaces of the disposal canister or migrate to the buffer material surrounding the disposal canister depending on their properties. They can undergo a sorption reaction with the buffer material. The penetration of such corrosion products into the buffer can contaminate the buffer and change its performance.

Under KURT conditions at 30 °C over 10 years, the Ca- and Na-type bentonite showed similar processes, such as continuous d-spacing expansion and CaO concentration increase. However, they also showed several differences. The Na_2O content of Na-bentonite (MX-80) decreased from 2.25% to 0.41–0.42%. These results suggest that the increase in the d-spacing of Na-bentonite was not simply due to a change in the two-layer hydration states without ion exchange but was caused by the replacement of the Na ions with Ca ions in the interlayer [33–35].

5. Conclusions

The increase in the d-spacing of Ca- and Na-bentonite is caused by the replacement of Na ions with Ca ions in the intermediate layer, as well as changes in the hydration state of the second layer without ion exchange. Whether Cu enters the interlayer via ion exchange should be studied further. Because no temperature changes were observed under an aerobic environment over 10 years, no changes were observed in the chemical and mineral compositions of the Ca- and Na-bentonite blocks. However, if the concentration of dissolved Cu cation increases as the temperature increases, Cu cations will tend to exchange ions with interlayer cations; therefore, the interlayer spacing of bentonite will change, resulting in the properties of the buffer material. The presence of either green Cu corrosion products or cuprite on the bentonite did not notably affect the porewater chemistry.

This study has some limitations. However, we believe that this study provides basic data for understanding the long-term stability and safety of deep geological disposal systems. We conducted experiments over 10 years in an underground research laboratory. We found that corrosion products were generated but the performance of the buffer material was maintained, thus indicating the long-term safety of deep geological disposal systems. However, as the experiment was conducted under aerobic conditions at 30 °C, it was difficult to determine the effect of sulfide. In future studies, we plan to interpret the results of an experiment conducted under anaerobic conditions at 70 °C. Future investigations into the effects of volume and density changes on the safety, performance, and radionuclide retardation ability of the buffer in relation to high temperatures are required.

Author Contributions: Conceptualization, M.L.; methodology, M.L.; formal analysis, M.K. and G.-Y.K. and J.J.; investigation, M.L.; resources, M.L. and G.-Y.K. and J.J.; data curation, M.K.; writing—original draft preparation, M.K.; writing—review and editing, M.K.; visualization, M.K.; supervision, J.-S.K.; project administration, J.-S.K.; funding acquisition, J.-S.K. All authors have read and agreed to the published version of the manuscript.

Funding: This work was supported by the Nuclear Research and Development Program of the National Research Foundation of Korea (2021M2E1A1085193).

Data Availability Statement: Not applicable.

Acknowledgments: The authors gratefully acknowledge the Nuclear Research and Development Program of the National Research Foundation of Korea. We would like to thank Chungbuk National University (CBNU) for assistance with FIB-EDS analysis, Korea Basic Science Institute (KBSI Ochang) for assistance with ICP-AES analysis, Korea Institute of Geoscience and Mineral Resources (KIGAM) for assistance with XRF and XRD analysis.

Conflicts of Interest: The authors declare no conflict of interest.

References

1. Dohrmann, R.; Kaufhold, S. Cation exchange and mineral reactions observed in MX80 buffer samples of the prototype repository in situ experiment in ASPO Sweden. *Clays Clay Miner.* **2014**, *62*, 357–373. [CrossRef]
2. Hadi, J.; Wersin, P.; Serneels, V.; Greneche, J.M. Eighteen years of steel-bentonite interaction in the FEBEX in situ test at the Grimsel Test Site in Switzerland. *Clays Clay Miner.* **2019**, *67*, 111–131. [CrossRef]
3. Fernández, A.M.; Marco, J.F.; Nieto, P.; León, F.J.; Robredo, L.M.; Clavero, M.Á.; Cardona, A.I.; Fernández, S.; Svensson, D.; Sellin, P. Characterization of bentonites from the in situ ABM5 heater experiment at Aspo Hard Rock Laboratory, Sweden. *Minerals* **2022**, *12*, 471. [CrossRef]
4. Karnland, O.; Olsson, S.; Nisson, U. *Mineralogy and Sealing Properties of Various Bentonites and Smectite Rich Clay Materials, Svensk Kärnbränslehantering AB Report, SKB. TR-06-30*; Swedish Nuclear Fuel and Waste Management Company: Stockholm, Sweden, 2006.
5. Lee, J.O.; Cho, W.J.; Kwon, S.K. Thermal-hydromechanical properties of reference bentonite buffer for a Korean HLW Repository. *Tunn. Undergr. Space* **2011**, *21*, 264–273.
6. Park, T.J.; Seoung, D. Thermal behavior of groundwater-saturated Korean buffer under the elevated temperature conditions: In-situ synchrotron X-ray powder diffraction study for the montmorillonite in Korean bentonite. *Nucl. Eng. Technol.* **2021**, *53*, 1511–1518. [CrossRef]
7. Salas, J.; Sena, C.; Arcos, D. Hydrogeochemical evolution of the bentonite buffer in a KBS-3 repository for radioactive waste. Reactive transport modelling of the LOT A2 experiment. *Appl. Clay Sci.* **2014**, *101*, 521–532. [CrossRef]
8. Siddiqua, S.; Blatz, J.; Siemens, G. Evaluation of the impact of pore fluid chemistry on the hydromechanical behaviour of clay-based sealing materials. *Can. Geotech. J.* **2011**, *48*, 199–213. [CrossRef]
9. Villar, M.V. Infiltration tests on a granite/bentonite mixture: Influence of water salinity. *Appl. Clay Sci.* **2006**, *31*, 96–109. [CrossRef]
10. Muhammad, N.; Siddiqua, S. Calcium bentonite vs sodium bentonite: The potential of calcium bentonite for soil foundation. *Mater. Today Proc.* **2022**, *48*, 822–827. [CrossRef]
11. Yoo, M.; Choi, H.J.; Lee, M.S.; Lee, S.Y. Measurement of properties of domestic bentonite for a buffer of an HLW Repository. *J. Nucl. Fuel Cycle Waste Technol.* **2016**, *14*, 135–147. [CrossRef]
12. Arcos, D.; Bruno, J.; Karnland, O. Geochemical model of the granite-bentonite-groundwater interaction at the Aspo HRL (LOT experiment). *Appl. Clay Sci.* **2003**, *23*, 219–228. [CrossRef]
13. Birgersson, M.; Karnland, O. Ion equilibrium between montmorillonite interlayer space and an external solution–consequences for diffusional transport. *Geochim. Cosmochim. Acta* **2009**, *73*, 1908–1923. [CrossRef]
14. Karnland, O. *Chemical and Mineralogical Characterization of the Bentonite Buffer for the Acceptance Control Procedure in a KBS-3 Repository, Svensk Kärnbränslehantering AB Report, SKB. TR-10-60*; Swedish Nuclear Fuel and Waste Management Company: Stockholm, Sweden, 2010.
15. Wan, Y.; Guo, D.; Hui, X.; Liu, L.; Yao, Y. Studies on hydration swelling and bound water type of sodium- and polymer-modified calcium bentonite. *Adv. Polym. Technol.* **2020**, *2020*, 9361795. [CrossRef]
16. Kaspar, V.; Sachlova, S.; Hofmanova, E.; Komarkova, B.; Havlova, V.; Aparicio, C.; Cerna, K.; Bartak, D.; Hlavackova, V. Geochemical, geotechnical and microbiological changes in Mg/Ca bentonite after thermal loading at 150 °C. *Minerals* **2021**, *11*, 965. [CrossRef]
17. Standish, T.; Chen, J.; Jacklin, R.; Jakupi, P.; Ramamurthy, S.; Zagidulin, D.; Keech, P.; Shoesmith, D. Corrosion of copper-coated steel high level nuclear waste containers under permanent disposal conditions. *Electrochim. Acta* **2016**, *211*, 331–342. [CrossRef]
18. King, F. *Corrosion of Copper in Alkaline Chloride Environments*; TR-02-25; Swedish Nuclear Fuel and Waste Management Co. (SKB): Stockholm, Sweden, 2002.
19. King, F.; Lilja, C.; Pederson, K.; Pitkanen, P.; Vahanen, M. *An Update of the State-of-the-Art Report on the Corrosion of Copper under Expected Conditions in a Deep Geological Repository, Eurajoki, Finland: Posiva Oy 2011–2001*; POSIVA, 2012; Swedish Nuclear Fuel and Waste Management Company: Stockholm, Sweden, 2010.
20. Smith, J.M. The Corrosion and Electrochemistry of Copper in Aqueous, Anoxic Sulphide Solutions. Ph.D. Thesis, University of Western Ontario, London, ON, Canada, 2007.
21. Smith, J.; Qin, Z.; King, F.; Werme, L.; Shoesmith, D.W. Sulphide film formation on copper under electrochemical and natural corrosion conditions. *Corrosion* **1997**, *63*, 135–144. [CrossRef]
22. Smith, J.; Qin, Z.; Shoesmith, D.W.; King, F.; Werme, L. Corrosion of copper nuclear waste containers in aqueous sulphide solutions. *Mater. Res. Soc. Symp. Proc.* **2004**, *824*, 45–50. [CrossRef]
23. Pusch, R.; Kasbohm, J.; Thao, H.T.M. Chemical stability of montmorillonite buffer clay under repository-like conditions-A synthesis of relevant experimental data. *Appl. Clay Sci.* **2010**, *47*, 113–119. [CrossRef]
24. Morton, J.D.; Semrau, J.D.; Hayes, K.F. An X-ray absorption spectroscopy study of the structure and reversibility of copper adsorbed to montmorillonite clay. *Geochim. Cosmochim. Acta* **2001**, *65*, 2709–2722. [CrossRef]
25. Strawn, D.G.; Palmer, N.E.; Furnare, L.J.; Goodell, C.; Amonette, J.E.; Kukkadapu, R.K. Copper sorption mechanisms on smectites. *Clays Clay Miner.* **2004**, *52*, 321–333. [CrossRef]
26. Undabeytia, T.; Nir, S.; Rytwo, G.; Serban, C.; Morillo, E.; Maqueda, C. Modeling adsorption-desorption processes of Cu on edge and planar sites of montmorillonite. *Environ. Sci. Technol.* **2002**, *36*, 2677–2683. [CrossRef]
27. Zhou, S.-W.; Xu, M.-G.; Ma, Y.-B.; Chen, S.-B.; Wei, D.-P. Aging mechanism of copper added to bentonite. *Geoderma* **2008**, *147*, 86–92. [CrossRef]

28. Xiao, G.; Xu, G.; Wei, T.; Zeng, J.; Liu, W.; Zhang, L. The effect of Cu (II) on swelling and shrinkage characteristics of sodium bentonite in landfills. *Appl. Sci.* **2021**, *11*, 3881. [CrossRef]
29. Lee, S.Y.; Lee, J.Y.; Jeong, J.; Kim, K. Characteristics for the copper exchange reaction by bentonite buffer. *J. Miner. Soc. Korea* **2014**, *27*, 293–299. [CrossRef]
30. Yoon, S.; Choo, Y.W. Evaluation on compression wave velocities and moduli of Gyeongju compacted bentonite. *J. Korean Geotech. Soc.* **2019**, *35*, 41–50.
31. Savage, D.; Arthur, R. *Exchangeability of Bentonite Buffer and Backfill Materials, STUK-TR 12*; Swedish Nuclear Fuel and Waste Management Company: Stockholm, Sweden, 2012.
32. Christidis, G.E.; Blum, A.E.; Eberl, D.D. Influence of layer charge and charge distribution of smectites on the flow behavior and swelling of bentnoites. *Appl. Clay Sci.* **2006**, *34*, 125–138. [CrossRef]
33. Christidis, G.E. The concept of layer charge of smectites and its implications for important smectite-water properties. *EMU Notes Mineral.* **2011**, *11*, 239–260.
34. Tao, L.; Xiao, T.F.; Yu, Z.; Tao, G. Swelling of K^+, Na^+ and Ca^{2+}-montmorillonites and hydration of interlayer cations: A molecular dynamics simulation. *Chin. Phys. B* **2010**, *19*, 109101. [CrossRef]
35. Yotsuji, K.; Tachi, Y.; Sakuma, H.; Kawamura, K. Effect of interlayer cations on montmorillonite swelling: Comparison between molecular dynamic simulations and experiments. *Appl. Clay Sci.* **2021**, *204*, 106034. [CrossRef]